Reaction Geometry and Thermostable Variant of Pyranose 2-Oxidase from the White-Rot Fungus *Peniophora* sp.[†,‡]

Michael Bannwarth,[§] Dorothée Heckmann-Pohl,[||] Sabine Bastian,[||] Friedrich Giffhorn,[||] and Georg E. Schulz*[,§]

Institut für Organische Chemie und Biochemie, Albert-Ludwigs-Universität, Albertstrasse 21, 79104 Freiburg im Breisgau, Germany, and Lehrstuhl für Angewandte Mikrobiologie, Universität des Saarlandes, Im Stadtwald, Gebäude A1.5, 66123 Saarbrücken, Germany

Received December 2, 2005; Revised Manuscript Received April 7, 2006

ABSTRACT: Pyranose 2-oxidase catalyzes the oxidation of a number of carbohydrates using dioxygen; glucose, for example, is oxidized at carbon 2. The structure of pyranose 2-oxidase with the reaction product 2-keto-β-D-glucose bound in the active center is reported in a new crystal form at 1.41 Å resolution. The binding structure suggests that the α-anomer cannot be processed. The binding mode of the oxidized product was used to model other sugars accepted by the enzyme and to explain its specificity and catalytic rates. The reported structure at pH 6.0 shows a drastic conformational change in the loop of residues 454−461 (loop 454−461) at the active center compared to that of a closely homologous enzyme analyzed at pH 4.5 with a bound acetate inhibitor. In our structures, the loop is highly mobile and shifts to make way for the sugar to pass into the active center. Presumably, loop 454−461 functions as a gatekeeper. Apart from the wild-type enzyme, a thermostable variant was analyzed at 1.84 Å resolution. In this variant, Glu542 is exchanged for a lysine. The observed stabilization could be a result of the mutated residue changing an ionic contact at a comparatively weak interface of the tetramer.

Pyranose 2-oxidase (P2ox,[1] pyranose:oxygen 2-oxidoreductase, EC 1.1.3.10) is produced by fungi (*1*). It catalyzes the oxidation of carbohydrates, mostly of pyranoses at the C2 position, giving rise to diketo sugars and hydrogen peroxide. A notable exception is L-sorbose which is oxidized at the C5 atom. The enzyme has been identified in approximately a dozen white-rot fungi species (*2*−*11*), which are the only organisms that completely decompose lignin (*12*). However, P2ox is also present in *Tricholoma matsutake* and *Lyophyllum shimeji*, which both belong to another group of fungi (*13*).

The structures of P2ox from the white-rot fungi *Trametes multicolor* (*10*) and *Peniophora* sp. (*11*) are known at 1.8 and 2.35 Å resolution, respectively. P2ox contains a FAD covalently linked to the His167 Nε2 atom of the polypeptide. It oxidizes glucose to reduce its FAD as shown in Figure 1. Reduced FAD subsequently converts dioxygen to hydrogen peroxide, which is then used by lignin peroxidase (*14*) or by manganese peroxidase (*15*) to produce oxygen radicals that degrade lignin (*12*). In some fungi, the oxidized sugar is further metabolized, for instance, to the antibiotic cortalcerone (*16*). P2ox is of technical interest because it can be used to synthesize various carbohydrate derivatives and also to produce rare sugars such as the noncaloric sweetener tagatose (*17*).

P2ox belongs to the glucose-methanol-choline (GMC) oxidoreductase family, which is part of the greater glutathione reductase family (*18*−*20*). At present, the structures of five GMC oxidoreductases are known: cholesterol oxidase (*21*, *22*), glucose oxidase (*23*, *24*), hydroxynitrile lyase related to an aryl alcohol oxidase (*25*), cellobiose dehydrogenase (*26*), and P2ox (*10*, *11*). Among them, only P2ox binds its FAD covalently. While P2ox is a tetramer, glucose oxidase is a dimer, and the other enzymes are monomeric. Ligated GMC enzyme structures are known for cholesterol oxidase with the bound substrate dehydroisoandrosterone (*27*), for cellobiose dehydrogenase with its inhibitor cellobiono-1,5-lactam (*28*), and for P2ox from *T. multicolor* with its weak inhibitor acetate (*10*). To date, no structure of P2ox with a substrate or substrate analogue bound to the active center has been published. Here we report two P2ox structures in a new crystal form at high resolution showing the wild-type enzyme with the bound reaction product 2-keto-β-D-glucose as well as a thermostable variant without ligand.

MATERIALS AND METHODS

Enzyme Production and Crystallization. Wild-type P2ox from *Peniophora* sp. and a thermostable enzyme variant carrying the E542K mutation (*29*, *30*) were produced in *Escherichia coli* BL21(DE3) and purified as described previously (*11*). The enzyme was then crystallized at 20 °C

[†] This work was supported by the Deutsche Forschungsgemeinschaft via Grant SFB-388 and by EU-NEPSA Contract QLK3-CT-2001-02400.

[‡] The atomic coordinates and structure factors have been deposited in the Protein Data Bank as entries 2F5V and 2F6C.

* To whom correspondence should be addressed: Institut für Organische Chemie und Biochemie, Albertstr. 21, D-79104 Freiburg im Breisgau, Germany. Telephone: +49 761 203-6058. Fax: +49 761 203-6161. E-mail: georg.schulz@ocbc.uni-freiburg.de.

[§] Albert-Ludwigs-Universität.

[||] Universität des Saarlandes.

[1] Abbreviations: *B*-factor, crystallographic temperature factor indicating atomic mobility; E542K, point mutation of glutamate to lysine at position 542 of the thermostable P2ox variant from *Peniophora* sp.; GMC oxidoreductases, family of enzymes related to the glucose, methanol, and choline oxidoreductases; P2ox, pyranose 2-oxidase.

10.1021/bi052465d CCC: $33.50
Published on Web 05/06/2006

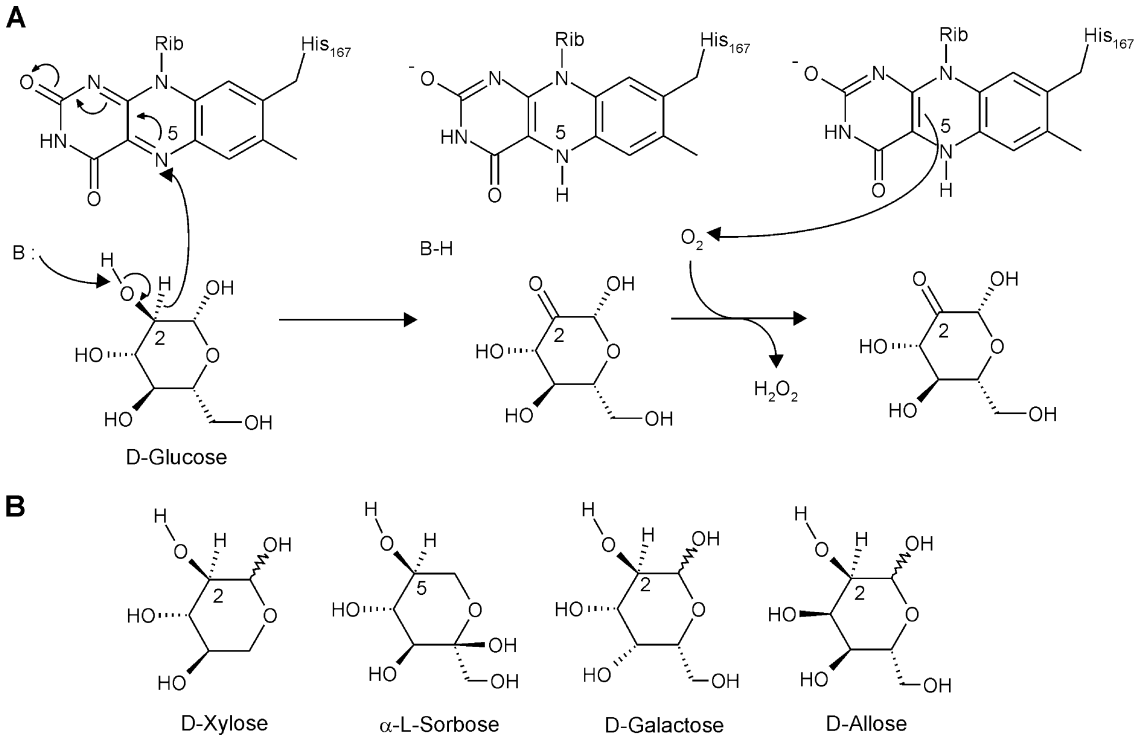

FIGURE 1: Catalytic reaction and substrates of P2ox. (A) Schematic representation of the reaction mechanism. Nϵ2 of His548 forms a hydrogen bond to the 2-hydroxyl group of D-glucose and most likely acts as the H^+-accepting base in the hydride transfer from C2 to the N5 atom of the flavin. The reduced flavin is reoxidized by dioxygen, giving rise to hydrogen peroxide. Flavin is covalently bound to Nϵ2 of His167. Most likely, the active center accepts only the β-anomer of D-glucose. (B) Four sugars processed by P2ox presented in the same orientation as 2-keto-β-D-glucose bound to the enzyme. The oxidized carbon is labeled. Enzyme kinetics data for these sugars are given in Table 3.

in 19% (w/v) PEG 6000, 100 mM MES (pH 6.0), and 4% (v/v) *n*-propanol which are essentially the same conditions used earlier (*11*). In this procedure, we obtained crystals belonging to space group $P4_22_12$ besides the previously reported $P2_1$ crystals (*11*). Focusing on the more suitable new crystal form, we collected data from a wild-type crystal with a size of $\sim$(200 μm)^3 that was soaked with 1 mM glucose for 3 min in cryo buffer [30% (w/v) PEG 6000, 15% 2-methyl-2,4-pentanediol, and 100 mM MES (pH 6.0)] and then shock-frozen at 100 K in a stream of cold nitrogen. The soak was performed in an aerobic environment. Subsequently, the crystal was cryo-annealed by blocking the cold stream for $\sim$15 s (*31*, *32*). Moreover, a crystal of the thermostable E542K variant was produced and handled in the same manner, except for the omission of *n*-propanol. However, neither was glucose was added nor cryo-annealing performed. The crystal was approximately the same size as that of the wild-type.

Data Collection and Structure Determination. X-ray diffraction data were collected at 100 K on beamline X11 of the EMBL outstation (Hamburg, Germany). The data were processed using XDS (*33*). The structure was determined by molecular replacement using the previously reported medium-resolution P2ox structure (*11*) as a search model in EPMR (*34*). The model was rebuilt with O (*35*) and ARP/wARP (*36*), followed by a refinement with REFMAC using the TLS method (*37*). The structure quality was monitored with PROCHECK (*38*). The parameter file for 2-keto-β-D-glucose was generated with PRODRG (*39*). Structures were superimposed with LSQMAN (*40*).

RESULTS AND DISCUSSION

Crystal Packing and Symmetry. The original structure was that of a selenomethionine-labeled P2ox with wild-type sequence at 2.35 Å resolution (*11*). The analyzed crystal belonged to space group $P2_1$ with two tetrameric molecules in the asymmetric unit. The crystals reported here contained the wild-type enzyme without the selenium label and the thermostable E542K variant. They grew under essentially the same conditions but belonged to space group $P4_22_12$ with a single subunit in the asymmetric unit. The highly symmetric $P4_22_12$ packing had already been detected as a pseudo-space group in the $P2_1$ crystals (*11*). Consequently, the enzyme assumed the same general packing arrangement in both crystal forms. However, the 119 Å long 4_2-axis reported here is 14 Å shorter than the pseudo-4-fold screw axis observed in the $P2_1$ crystal. This corresponds to the change of the solvent contents from 50% in the $P2_1$ crystal to 47% in the crystals belonging to space group $P4_22_12$.

The diffraction power of the produced crystals varied greatly and could not be reproduced, both at room temperature and after shock-freezing to 100 K. It ranged between almost no diffraction at all and reflections to 2 Å resolution. Conceivably, the crystals grew as some mixture of the closely related $P2_1$ and $P4_22_12$ packing schemes lacking internal order. Therefore, as a simple method, we tried cryo-annealing to obtain uniform crystals (*31*, *32*). With most P2ox crystals, cryo-annealing decreased the diffraction power. However, we succeeded in inducing one particular crystal, also soaked with glucose, to assume a well-ordered packing, which yielded high-resolution X-ray diffraction data (Table 1). In

Table 1: Data Collection and Refinement Statistics of a Complex between Wild-Type P2ox and 2-Keto-β-D-glucose and the Thermostable E542K Variant[a]

	complex	E542K variant
resolution (Å)	62−1.41 (1.47−1.41)	77−1.84 (1.90−1.84)
no. of unique reflections	119166	54750
completeness (%)	97.6 (80)	100 (100)
R_{sym-I} (%)	5.8 (38)	9.4 (34)
multiplicity	15.8 (14.1)	8.0 (8.1)
average I/σ_I	27.0 (7.3)	15.9 (6.1)
no. of atoms		
polypeptides	4550	4550
FADs	53	53
sugars	12	−
water molecules	800	595
average *B*-factor (Å^2)		
main chain	12.8	8.0
side chains	15.2	9.9
rmsd		
bond lengths (Å)	0.015	0.015
bond angles (deg)	1.6	1.5
R_{cryst} (%)	14.9	15.2
R_{free} (%)	17.8	18.6
Ramachandran plot (%)		
most favored	90.2	90
others	9.8	10

[a] All data were collected at 100 K on beamline X11 of the EMBL outstation using a wavelength of 0.8123 Å. Both crystals belong to space group $P4_22_12$ with one subunit per asymmetric unit. The cell axes were as follows for the complex: $a = b = 102.2$ Å and $c = 119.9$ Å. They were as follows for the variant: $a = b = 101.9$ Å and $c = 118.6$ Å. The test sets for R_{free} were 2 and 5% for the complex and the variant, respectively.

some respects, our cryo-annealing trials are reminiscent of dehydration experiments, which in several instances also improved protein crystal ordering (*41*). Actually, dehydration may also happen during cryo-annealing. The crystal of the thermostable E542K variant was isomorphous to that of wild-type P2ox and well-ordered without cryo-annealing. The collected X-ray diffraction data of both crystals were of high quality (Table 1).

Protein Structure. P2ox is a D_2-symmetric homotetramer (Figure 2A). It contains a large internal cavity at its center of symmetry (*10*, *11*). This cavity functions as a vestibule, through which the sugars have to pass to reach the four active centers. Since the vestibule has to be entered through narrow pores (*11*), P2ox cannot oxidize large substrates such as glycoproteins. Each subunit of the crystallized tetramer consisted of 595 amino acid residues and one covalently bound FAD with a total mass of 67 225 Da. The tetramer is best described as a weakly associated dimer of the two tight dimers, S-U and T-V, shown in Figure 2A, the tight interface having almost twice the area of the weak interface (*11*).

The two reported crystal structures were elucidated using the molecular replacement method and subsequently refined (Table 1). One structure shows the wild-type enzyme in complex with the reaction product 2-keto-β-D-glucose in the active center. The other structure is that of the thermostable E542K variant without a ligand. The two chain folds correspond closely to each other. The rmsd of the Cα atoms is merely 0.13 Å with maximum deviations of 0.7 Å. The two *B*-factor plots were identical to each other and also essentially identical to the *B*-factor plots of the $P2_1$ crystal published previously (*11*).

However, conformational changes emerged when comparing the two reported $P4_22_12$ crystal structures with the eight crystallographically independent subunit structures of the $P2_1$ crystal (*11*). Appreciable differences occur in the "dimer loop" (rmsd of the Cα atoms of up to 1.1 Å), the "protrusion" (rmsd of the Cα atoms of up to 1.5 Å), the mobile loop of residues 341−346 on the outer surface (rmsd of the Cα atoms of up to 0.6 Å), and the mobile loop of residues 454−461 near the active center (Figure 2B). Loop 454−461 most likely functions as a gatekeeper for the active center (see below) and is therefore of special interest. A superposition of the wild-type tetramer of the $P4_22_12$ crystal with the two independent tetramers of the $P2_1$ crystal (*11*) shows an overall shrinkage of the $P4_22_12$ tetramer in relation to the two $P2_1$ tetramers. The shrinkage is in the range of 1 Å and is probably caused by differences in the crystal contacts. It indicates that the subunits could move slightly relative to each other.

The P2ox tetramer is a weakly associated dimer of the tight dimers S-U and T-V (Figure 2). Interestingly, the D_2 symmetry of the tetramer is broken locally in the $P2_1$ crystals where the two contacting atoms, Asp81 O and Asp81′ O, in the tight dimer interface are not symmetric (*11*). A comparison with the closely homologous P2ox from *T. multicolor* (*10*), which crystallized with one tetramer in the crystallographic asymmetric unit, reveals the same local symmetry violation. This violation is also supported by the structures in the $P4_22_12$ crystals where the enforced symmetry resulted in a collision (Figure 3A). In all instances, the violation reduced the tetramer symmetry from point group D_2 to C_2 rather than completely destroying it. In conclusion, the symmetry violation reveals tetramer states differing from each other in slight subunit rearrangements. Such states may be interconverted during the reaction and may therefore affect the catalysis.

Active Center. The reported wild-type $P4_22_12$ crystal contained electron density for a sugar molecule with less than full occupancy at the *re* face of the flavin (Figure 4A). Assuming uniform *B*-factors of the sugar and surrounding protein, the occupation was ∼50%. The atomic contacts of the bound sugar are listed in Table 2. As shown in panels B and C of Figure 4, the electron density clearly fits the oxidized reaction product 2-keto-β-D-glucose and not the educt D-glucose. Therefore, we conclude that the crystalline enzyme is active, which seems reasonable as the active center is completely buried within the tetramer. Moreover, given the free access of air, the 3 min soaking time permitted more than 1000 turnovers (Table 3), which should have sufficed to oxidize all bound glucose. We suggest that the bound sugar was fixed by shock-freezing to 100 K and that the sugar and the flavin were then completely oxidized by dioxygen, which retained some mobility even at rather low temperatures. Activity in an enzyme crystal resulting in the product of the catalyzed reaction has been observed elsewhere (*42*). The crystal color remained yellow over the soaking time, indicating that dioxygen reoxidized flavin fast enough to prevent the accumulation of reduced FAD.

Besides the bound product, some additional diffuse density between the ring oxygen of the product (O5) and Phe454 cannot be explained by discrete water molecules (Figure 4A). We suggest that this density represents a mixture of water and trapped hydrogen peroxide. Interestingly, mobile loop

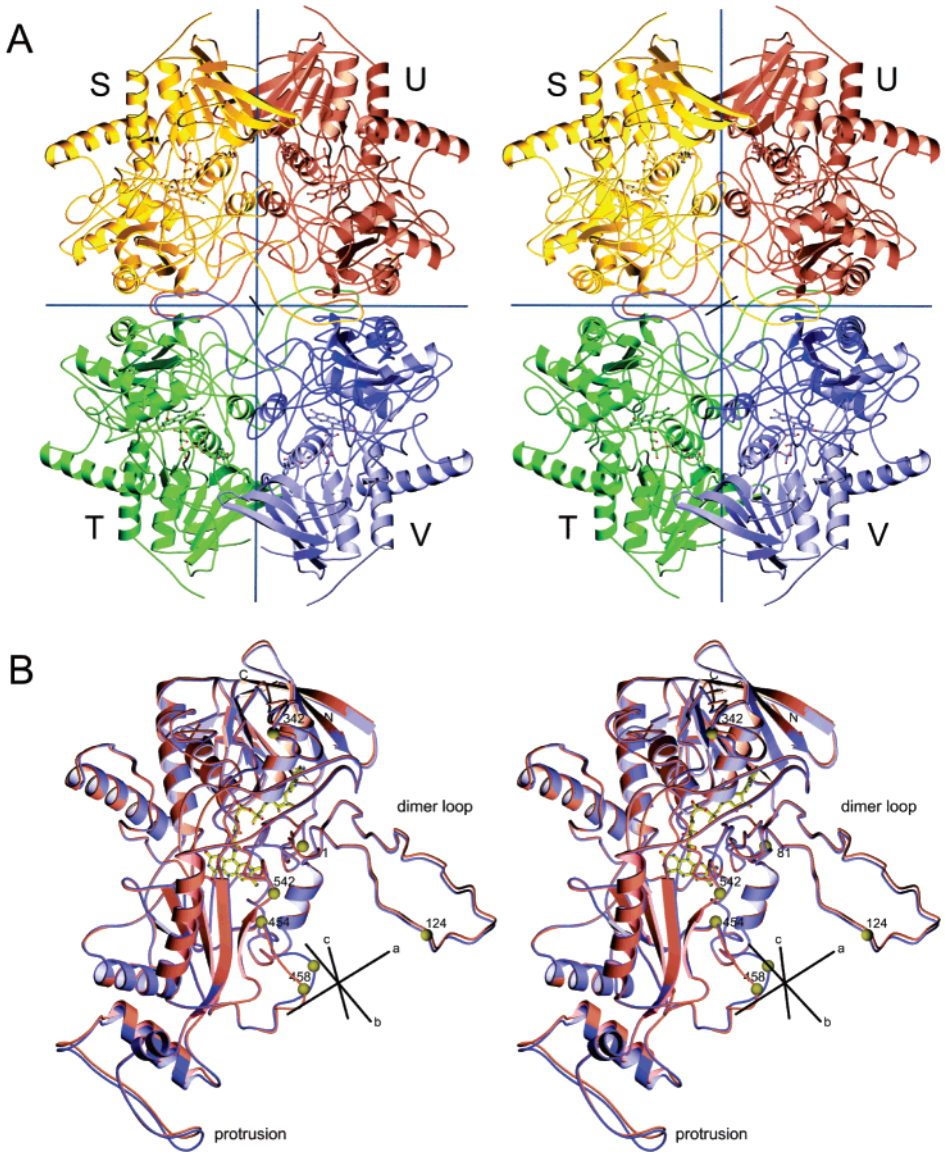

FIGURE 2: Ribbon plots showing the chain fold of P2ox. (A) Stereoview of the D_2-symmetric tetrameric enzyme. The view is along the *a*-axis; the *c*-axis is vertical. The vestibule is at the center. The FAD molecules are given as ball-and-stick models. The tight interfaces are between subunits S and U as well as between T and V. The weak interfaces are between S and T as well as between U and V. (B) Stereoview of a chain fold comparison between wild-type P2ox in space group $P4_22_12$ (blue) and selenomethionine-labeled P2ox in space group $P2_1$ (red) (*11*). There are appreciable variations between the eight crystallographically independent subunits in the $P2_1$ crystal. According to LSQMAN (*40*), chain E is closest to the average and was therefore used here as the representative of all subunits in the $P2_1$ crystal. The chain fold of the thermostable variant E542K in a $P4_22_12$ crystal is not shown because it is very similar to that of wild-type P2ox in the same crystal form. The structures differ from each other at the extended dimer loop (residues 115−148), at loop 341−346, at the protrusion (residues 372−427), and with respect to loop 454−461 at the entrance to the active center pocket. The protrusion is at the surface of the tetramer. The dimer loop fastens the tight S−U and T−V dimers around the *c*-axis. Asp81, Asp124, Pro342, Phe454, Ala458, and Glu542 are depicted as yellow spheres. Asp81 at the *c*-axis shows a local symmetry violation (Figure 3A). The substituted position 542 of the thermostable variant contacts Asp124 on the dimer loop across the weak S−T and U−V interfaces (Figure 3A).

454−461 at the active center assumes essentially the same conformation in the complex as in the substrate-free thermostable variant and in the previously reported substrate-free $P2_1$ crystal (*11*). Merely Phe454, which has to move away during sugar passage, undergoes a slight side chain displacement (Figure 5A).

The binding structure of 2-keto-β-D-glucose in the active center makes it very unlikely that the enzyme accepts the α-anomer, because the respective 1-hydroxyl group would collide severely with Val546 and Phe474 (Figure 5A). The ignored α-anomer should therefore accumulate in the central cavity of the tetramer, i.e., the vestibule (Figure 2A). It seems likely that the concave lining of the vestibule could facilitate a mutarotation reaction recovering the α-anomer. The only residues that could serve as the catalytic base in the vestibule are Asp124 and Glu542 shown in Figure 3B.

Thermostable Variant. The P2ox variant carrying the E542K mutation exhibits an improved thermostability at neutral pH as the temperature of inactivation increases by 20 °C and the temperature of optimal activity by ~5 °C (*29*, *30*, *43*). Residue 542 is part of the weak interface between subunits S and T (U and V) contacting Asp124′ of the dimer loop (Figure 2B). The dimer loop makes up a large part of the weak interface but also contributes appreciably to the tight dimer interface between S and U (T and V). Residue 542 and Asp124′ are at the surface of the large inner cavity,

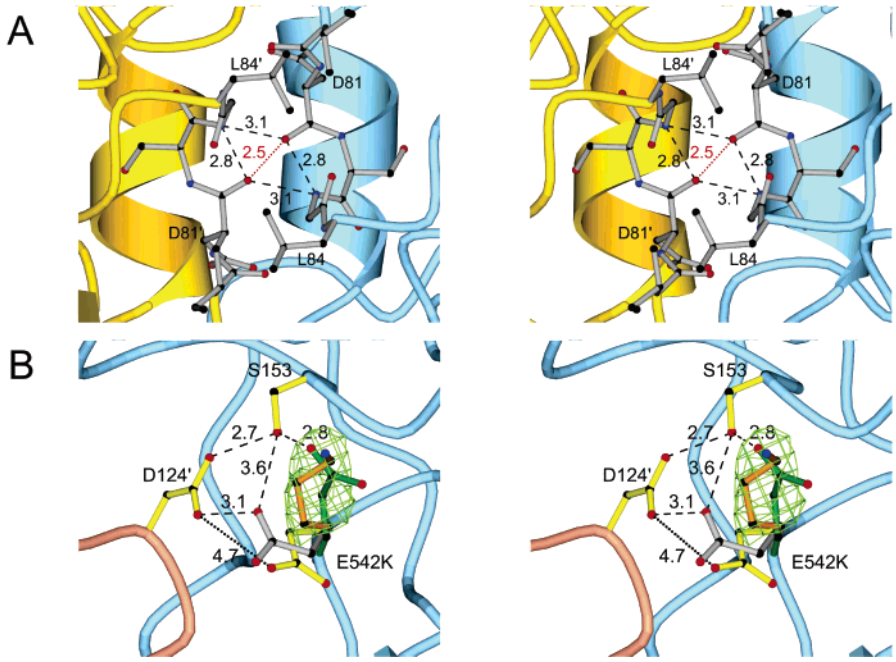

FIGURE 3: Stereoview of interface contacts in the P2ox tetramer. (A) In the $P4_22_12$ crystals, the contact between O of Asp81 and O of Asp81′ shows a collision across the *c*-axis. This contact is in the tight interface between subunits S and U (T and V) (Figure 2). In the $P2_1$ crystals without the enforced D_2 symmetry of the $P4_22_12$ crystal, the carbonyl oxygens avoid each other causing a local symmetry violation. (B) $F_o - F_c$ difference electron density of the thermostable variant carrying the E542K mutation. The density is depicted at the 3.0σ contour level. There is no significant negative density. F_c was calculated using the main chain and the Cβ atom of residue 542. The electron density supports the assigned position for the lysine side chain (orange). The view is from the vestibule at the tetramer center. The wild-type structure in the $P4_22_12$ crystal at pH 6.0 shows Glu542 turning away (yellow). In the $P2_1$ crystals at pH 6.0, this conformation is also assumed by four of the eight crystallographically independent Glu542 residues (yellow), while the gray conformation is found in three instances. The green conformation is observed once in the $P2_1$ crystals and also in all four independent Glu542 residues of the P2ox from *T. multicolor* that was analyzed at pH 4.5 (*10*).

Table 2: Contacts between Wild-Type P2ox and the Bound 2-Keto-β-D-glucose Molecule

2-ketoglucose	contacting atom	distance (Å)	interaction type
C1	Val546 Cγ2	4.5	nonpolar
O1	Val546 O	2.7	hydrogen bond
O1	Leu547 Cβ	4.5	polar−nonpolar
C2	flavin N5	3.2	hydride transfer
O2	His548 Nϵ2	2.7	hydrogen bond
O2	Asn593 Nϵ2	2.8	hydrogen bond
C3	Phe474 Cζ	3.6	nonpolar
O3	flavin O4	2.8	hydrogen bond
O3	Gln448 Nϵ2	3.0	hydrogen bond
O3	Asn593 Nϵ2	3.1	hydrogen bond
C4	Thr169 Cβ	3.9	nonpolar
O4	Arg472 Cδ	3.4	polar−nonpolar
O4	Asp452 Oδ2	2.6	hydrogen bond
O4	Gln448 Nϵ2	3.1	hydrogen bond
O4	His450 Nϵ2	3.5	hydrogen bond
C5	Leu361 Cδ2	5.7	nonpolar
O6	Phe454 Cβ	3.8	polar−nonpolar
O6	Asp452 Oδ1	2.9	hydrogen bond
O6	Thr169 Oγ1	3.3	hydrogen bond

Table 3: Published Enzyme Kinetic Data of P2ox[a]

	T. multicolor[b]		*P. gigantea*[b]		*Peniophora* sp.[c]	
substrate	k_{cat} (s^{-1})	K_m (mM)	k_{cat} (s^{-1})	K_m (mM)	k_{cat} (s^{-1})	K_m (mM)
D-glucose	54	0.74	56	1.1	9.4	5
L-sorbose[d]	53	38	42	50	2.2	42
D-xylose	30	30	23	29	1.3	40
D-allose	20	36	16	56	nd	nd
D-galactose	3.1	9.2	2.8	8.2	nd	nd
D-melibiose	8.6	120	—[e]	—[e]	nd	nd

[a] All data were determined using the chromogenic ABTS assay (*5*). [b] The data of *T. multicolor* (*9*) and *P. gigantea* (*30*) were determined using the native enzymes directly isolated from the fungi. [c] The data are from the recombinant enzyme with the wild-type sequence (*43*) that has been used in the structure analysis. The sequences of P2ox from *Peniophora* sp. are 99% identical to those from *T. multicolor* and 83% identical to those from *P. gigantea*. [d] In solution, 98% of L-sorbose is α-L-sorbosepyranose and 2% is β-L-sorbosepyranose (*48*). [e] A test showed no significant activity above the detection level (*50*).

called here the vestibule, ~10 Å from the entrance to the active center pocket.

As shown in Figure 3B, the newly introduced lysine side chain is well-ordered, exhibiting a *B*-factor of 19 Å^2 for its Nζ atom, although it does not bind directly to any other part of the protein. The distance between the Nζ atom and Oδ1 of Asp124′ is 6.5 Å. At neutral pH, Lys542 abolishes the destabilizing repulsion between Asp124′ and Glu542 of the wild type. Accordingly, the structure explains the increased temperature stability observed at normal pH (*30*, *43*). In contrast, at low pH, the carboxylates of wild-type P2ox may form a strong hydrogen bond with each other, stabilizing the enzyme. The observation that oligomeric enzymes are stabilized by mutations at an interface is well-known from other enzymes (*44*, *45*).

The local structure around residue 542 varies greatly. P2ox from *T. multicolor* was crystallized at a low pH of 4.5 and exhibited identical conformations in all four crystallographically independent sites (Figure 3B). In this species, Asp124′ of the dimer loop forms a hydrogen bond to Ser153 of the adjacent subunit, which is backed up by a hydrogen bond to Glu542 of the same subunit. In contrast, the crystals of P2ox from *Peniophora* sp. were at pH 6.0. All of them showed

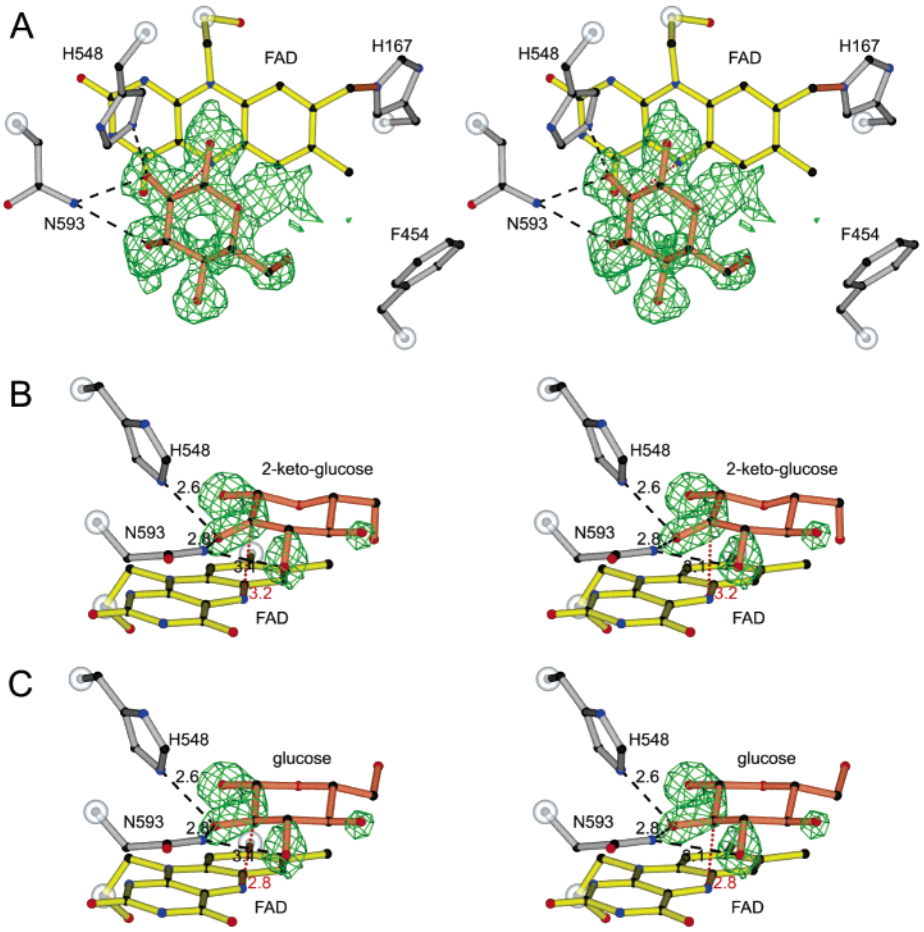

FIGURE 4: Stereoview of the complex between wild-type P2ox and the reaction product 2-keto-β-D-glucose analyzed at 1.41 Å resolution in a $P4_22_12$ crystal. (A) $F_o - F_c$ difference electron density at the 2.5σ contour level in the active center. The refined model of 2-keto-β-D-glucose is drawn in this electron density. The occupancy is ~50%. (B) $F_o - F_c$ difference electron density at the very high 5.0σ level, demonstrating that educt β-D-glucose does not fit the density. Actually, a separate refinement with the educt resulted in unexplained positive density above the C2 atom at the α-side of the sugar, which confirms the interpretation as a 2-keto group. (C) The same density as in panel B with a model of the reaction product 2-keto-β-D-glucose shows a very good fit.

the hydrogen bond between Asp124′ and Ser153. However, Glu542 was turned away in the $P4_22_12$ crystal as well as in four of the eight independent subunits of the $P2_1$ crystal (*11*). In three subunits of the $P2_1$ crystal, Glu542 formed a hydrogen bond to Asp124′ and in one instance a hydrogen bond to Ser153 like that at pH 4.5 (Figure 3B). The observed structural variations indicate that the E542K mutation is located at a critical point of the weak interface between the tight dimers that may be important for subunit rearrangements. Interestingly, variant E542K exhibits approximately twice the activity of the wild type (*43*), which may be related to a deviating subunit association behavior during catalysis. It should be kept in mind, however, that the E542K mutation may also affect the proposed mutarotation in the vestibule.

Specificity and Reaction Mechanism. The 2-keto-β-D-glucose model of Figure 5 is defined by the experimental density shown in Figure 4. Moreover, it is supported by the abundance of hydrogen bonds with the polypeptide and by the suitably positioned C2 atom at the flavin N5 atom (Table 2). In general terms, it also corresponds to the position of the inhibitor cellobiono-1,5-lactam bound to the homologous enzyme cellobiose dehydrogenase (*28*), which had been aligned with P2ox before (*11*). Phe474 forms a tight 3.8 Å nonpolar contact with the α-face of the glucose pushing the sugar toward the flavin. Phe474 is strictly conserved in all enzymes of the P2ox family. Phe454 of the gatekeeper loop closes like a lid on the substrate and is mobile (Figure 5).

Most likely, P2ox catalyzes the oxidation of glucose by a hydride transfer mechanism. The hydride ion travels from C2 to the N5 atom of the flavin as indicated in Figures 1 and 5A. The C2 atom is polarized by hydrogen bonds between the 2-hydroxyl group and Asn593 as well as His548, among which His548 most likely functions as the base accepting the proton concomitantly transferred with the hydride. This assumption is corroborated by the strict conservation of His548 (P2ox) as His447 of cholesterol oxidase (*21*, *22*), as His516 of glucose oxidase (*46*), as His459 of hydroxynitrile lyase (*25*), and as His689 of cellobiose dehydrogenase (*28*). The role of this histidine as a base facilitating oxidation has been questioned for cholesterol oxidase, where the spatially adjacent Glu361 may abstract the proton as well and where a 0.95 Å resolution structure at pH 5.2 was interpreted in terms of a protonated His447 (*47*). However, the proposed proton at His447 cannot be considered secure. Moreover, the pH of 5.2 used in the analysis is almost 1 pH unit below the usual pK_a of an imidazole and almost 2 pH units below the pH used in the cholesterol oxidase assay (*22*). As a consequence, the discussion about cholesterol oxidase does not appear to be relevant for P2ox.

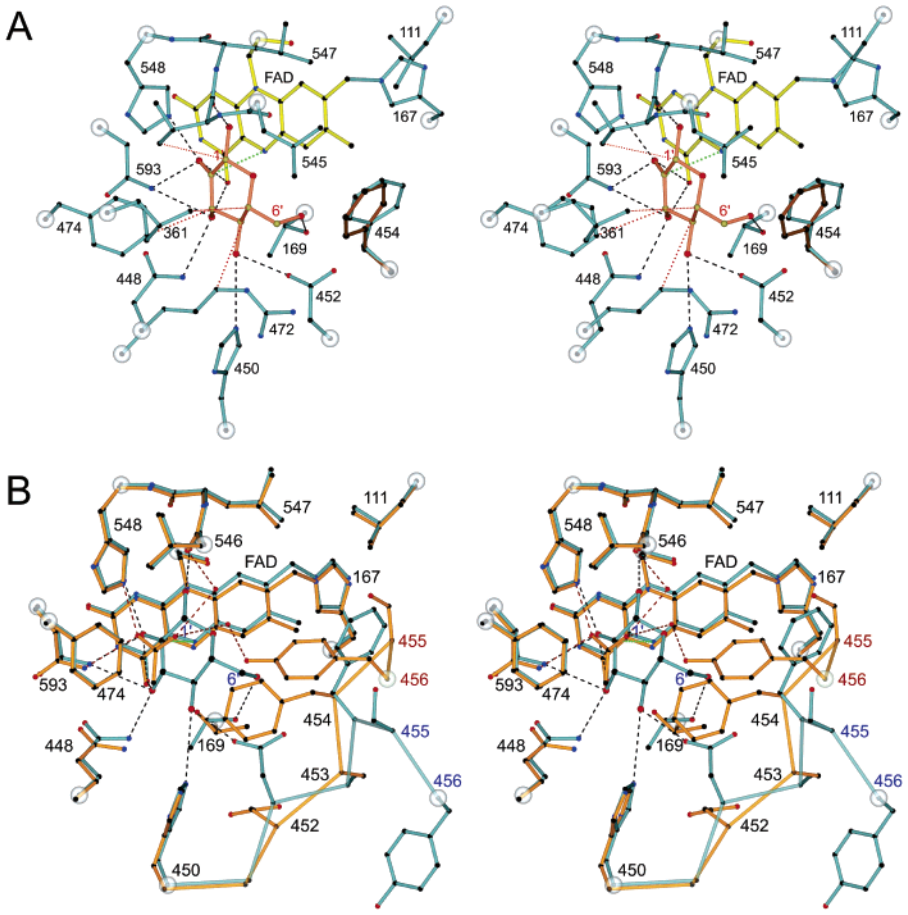

FIGURE 5: Stereoview of the active center. Chain cuts are marked with halos. (A) Binding structure of 2-keto-β-D-glucose in the $P4_22_12$ crystal, including all residues involved in hydrogen bonds (dashed lines) or other interactions (dotted lines). The distances are listed in Table 2. The conformation of Phe454 differs from those observed in the $P2_1$ crystal (brown), which also vary appreciably among themselves. Chain E of the $P2_1$ crystal was chosen as the representative (see Figure 2). (B) Superposition of the active centers of native P2ox from *Peniophora* sp. with bound 2-keto-β-D-glucose at pH 6.0 (blue) and P2ox from *T. multicolor* at pH 4.5 containing a bound acetate inhibitor with a K_i of 9.2 mM (orange) (*10*). The view is from the large central cavity of the tetramer into the active center pocket. Several residues have been omitted for the sake of clarity. Note the large conformational difference in gatekeeper loop 454−461.

The polar environment provides enough hydrogen bonding options to allow the weak binding of sugars other than glucose. For example, the missing 6-hydroxymethyl group in D-xylose with respect to D-glucose (Figure 1B) causes only a small decrease in the catalytic rate of the homologous enzymes from *T. multicolor* and *Peniophora gigantea* as stated in the published data in Table 3. However, it raises the Michaelis constant K_m appreciably, indicating much weaker binding. The importance of this hydroxymethyl group is also indicated by the oxidation of α-L-sorbose at the C5 position. Here, we consider only the α-anomer because it is the dominant (98%) form in solution (*48*). As shown in Figure 1B, the 1-hydroxymethyl group of the sorbose most likely occupies the position of the 6-hydroxymethyl of glucose, bringing the C5 atom into a position to be oxidized. The increase in the K_m value of α-L-sorbose (Table 3) is explained by the collision of its 2-hydroxyl group with the side chain of Leu361 (Figure 5A).

The axial 3-hydroxyl group of D-allose requires a shift of Phe474, which may be facilitated by interactions with Gln448 and Asn593. This increases the Michaelis constant greatly (Table 3). On the other hand, the 2 position is not very much affected, limiting the decrease in the reaction rate. The structure of the fitted D-glucose explains why P2ox is not reactive against D-mannose. With D-mannose, the axial 2-hydroxyl group, and not the C2 atom, would point to the flavin N5 atom prohibiting a hydride transfer. Galactose with its 4-hydroxyl group in the axial position shows a moderate increase in the K_m value but a considerable decrease in the catalytic rate (Table 3). Presumably, this 4-hydroxyl group forms hydrogen bonds to Oδ2 of Asp452 and Oγ of Thr169 as visualized in Figure 5A. These bonds may shift the pyranose ring somewhat out of the optimal position for hydride transfer, causing the diminished reaction rate (Table 3). Since the 6-hydroxymethyl group of glucose is located in the entrance region of the active center, 6-O-linked carbohydrates such as the disaccharides D-melibiose and D-α-1,6-isomaltose can be accommodated if gatekeeper loop 454−461 is displaced. Actually, these compounds were shown to be processed by P2ox from *T. multicolor*, though at a very low rate (Table 3).

A comparison with the structure of P2ox from *T. multicolor* shows a generally close correspondence except for the active center. The *T. multicolor* enzyme was crystallized at pH 4.5, revealing one acetate molecule of the buffer bound at the main sugar site in front of the flavin. This acetate and the low pH seem to have caused a dramatic conformational change of mobile gatekeeper loop 454−461, drawing Phe454 and Tyr456 deep into the active center and thus clogging the pocket and entrance. The conformational difference is

depicted in Figure 5B. It confirms that the loop is highly mobile and that it moves during the substrate passage. For such a passage, a widening of the pocket entrance of the *Peniophora* sp. structures is necessary. The passage is probably facilitated by transient interactions of Phe454 and also Tyr456 with the nonpolar sugar faces (*49*). The extensive conformational change of the gatekeeper loop provides another example of the common observation that multiple crystal structures may be most helpful in exploring catalytic processes.

ACKNOWLEDGMENT

We thank the team of the EMBL-outstation Hamburg for their help with data collection.

REFERENCES

1. Giffhorn, F. (2000) Fungal pyranose oxidases: Occurrence, properties and biotechnical applications in carbohydrate chemistry, *Appl. Microbiol. Biotechnol. 54*, 727−740.
2. Janssen, F. W., and Ruelius, H. W. (1975) Pyranose oxidase from *Polyporus obtusus*, *Methods Enzymol. 41*, 170−173.
3. Machida, Y., and Nakanishi, T. (1984) Purification and properties of pyranose oxidase from *Coriolus versicolor*, *Agric. Biol. Chem. 48*, 2463−2470.
4. Volc, J., Denisova, N. P., Nerud, F., and Musilek, V. (1985) Glucose-2-oxidase activity in mycelial cultures of basidiomycetes, *Folia Microbiol. (Prague, Czech Repub.) 30*, 141−147.
5. Danneel, H. J., Rossner, E., Zeeck, A., and Giffhorn, F. (1993) Purification and characterization of a pyranose oxidase from the basidiomycete *Peniophora gigantea* and chemical analyses of its reaction products, *Eur. J. Biochem. 214*, 795−802.
6. Daniel, G., Volc, J., and Kubatova, E. (1994) Pyranose oxidase, a major source of H_2O_2 during wood degradation by *Phanerochaete chrysosporium*, *Trametes versicolor* and *Oudemansiella mucida*, *Appl. Environ. Microbiol. 60*, 2524−2532.
7. Schäfer, A., Bieg, S., Huwig, A., Kohring, G. W., and Giffhorn, F. (1996) Purification by immunoaffinity chromatography, characterization, and structural analysis of a thermostable pyranose oxidase from the white rot fungus *Phlebiopsis gigantea*, *Appl. Environ. Microbiol. 62*, 2586−2592.
8. Artolozaga, M. J., Kubatova, E., Volc, J., and Kalisz, H. M. (1997) Pyranose 2-oxidase from *Phanaerochaete chrysosporium*: Further biochemical characterization, *Appl. Microbiol. Biotechnol. 47*, 508−514.
9. Leitner, C., Volc, J., and Haltrich, D. (2001) Purification and characterization of pyranose oxidase from the white rot fungus *Trametes multicolor*, *Appl. Environ. Microbiol. 67*, 3636−3644.
10. Hallberg, B. M., Leitner, C., Haltrich, D., and Divne, C. (2004) Crystal structure of the 270 kDa homotetrameric lignin-degrading enzyme pyranose 2-oxidase, *J. Mol. Biol. 341*, 781−796.
11. Bannwarth, M., Bastian, S., Heckmann-Pohl, D., Giffhorn, F., and Schulz, G. E. (2004) Crystal structure of pyranose 2-oxidase from the white rot fungus *Peniophora* sp., *Biochemistry 43*, 11683−11690.
12. ten Have, R., and Teunissen, P. J. M. (2001) Oxidative mechanisms involved in lignin degradation by white-rot fungi, *Chem. Rev. 101*, 3397−3413.
13. Takakura, Y., and Kuwata, S. (2003) Purification, characterization, and molecular cloning of a pyranose oxidase from the fruit body of the basidiomycete, *Tricholoma matsutake*, *Biosci., Biotechnol., Biochem. 67*, 2598−2607.
14. Edwards, S. L., Raag, R., Wariischi, H., Gold, M. H., and Poulos, T. L. (1993) Crystal structure of lignin peroxidase, *Proc. Natl. Acad. Sci. U.S.A. 90*, 750−754.
15. Sundaramoorthy, M., Kishi, K., Gold, M. H., and Poulos, T. L. (1994) The crystal structure of manganese peroxidase from *Phanerochaete chrysosporium* at 2.06 Å resolution, *J. Biol. Chem. 269*, 32759−32767.
16. Koths, K., Halenbeck, R., and Moreland, M. (1992) Synthesis of the antibiotic cortalcerone from D-glucose using pyranose 2-oxidase and a novel fungal enzyme, aldos-2-ulose dehydratase, *Carbohydr. Res. 232*, 59−75.
17. Freimund, S., Huwig, A., Giffhorn, F., and Köpper, S. (1996) Convenient chemo-enzymatic synthesis of D-tagatose, *J. Carbohydr. Chem. 15*, 115−120.
18. Schulz, G. E., Schirmer, R. H., Sachsenheimer, W., and Pai, E. F. (1978) The structure of the flavoenzyme glutathione reductase, *Nature 273*, 120−124.
19. Cavener, D. R. (1992) GMC oxidoreductases. A newly defined family of homologous proteins with diverse catalytic activities, *J. Mol. Biol. 223*, 811−814.
20. Dym, O., and Eisenberg, D. (2001) Sequence-structure analysis of FAD-containing proteins, *Protein Sci. 10*, 1712−1728.
21. Vrielink, A., Lloyd, L. F., and Blow, D. M. (1991) Crystal structure of cholesterol oxidase from *Brevibacterium sterolicum* refined at 1.8 Å resolution, *J. Mol. Biol. 219*, 533−554.
22. Yue, Q. K., Kass, I. J., Sampson, N. S., and Vrielink, A. (1999) Crystal structure determination of cholesterol oxidase from *Streptomyces* and structural characterization of key active site mutants, *Biochemistry 38*, 4277−4286.
23. Hecht, H. J., Kalisz, H. M., Hendle, J., Schmid, R. D., and Schomburg D. (1993) Crystal structure of glucose oxidase from *Aspergillus niger* refined at 2.3 Å resolution, *J. Mol. Biol. 229*, 153−172.
24. Wohlfahrt, G., Witt, S., Hendle, J., Schomburg, D., Kalisz, H. M., and Hecht, H. J. (1999) 1.8 and 1.9 Å resolution structures of *Penicillium amagasakiense* and *Aspergillus niger* glucose oxidases as a basis for modelling substrate complexes, *Acta Crystallogr. D55*, 969−977.
25. Dreveny, I., Gruber, K., Glieder, A., Thompson, A., and Kratky, C. (2001) The hydroxynitrile lyase from almond: A lyase that looks like an oxidoreductase, *Structure 9*, 803−815.
26. Hallberg, B. M., Henriksson, G., Pettersson, G., and Divne, C. (2002) Crystal structure of the flavoprotein domain of the extracellular flavocytochrome cellobiose dehydrogenase, *J. Mol. Biol. 315*, 421−434.
27. Li, J., Vrielink, A., Brick, P., and Blow, D. M. (1993) Crystal structure of cholesterol oxidase complemented with a steroid substrate: Implications for flavine adenine dinucleotide dependent alcohol dehydrogenases, *Biochemistry 32*, 11507−11515.
28. Hallberg, B. M., Henriksson, G., Petterson, G., Vasella, A., and Divne, C. (2003) Mechanism of the reductive half-reaction in cellobiose dehydrogenase, *J. Biol. Chem. 278*, 7160−7166.
29. Masuda-Nishimura, I., Minamihara, T., and Koyama, Y. (1999) Improvement in thermal stability and reactivity of pyranose oxidase from *Coriolus versicolor* by random mutagenesis, *Biotechnol. Lett. 21*, 203−207.
30. Bastian, S., Rekowski, M. J., Witte, K., Heckmann-Pohl, D. M., and Giffhorn, F. (2005) Engineering of pyranose 2-oxidase from *Peniophora gigantea* towards improved thermostability and catalytic efficiency, *Appl. Microbiol. Biotechnol. 67*, 654−663.
31. Yeh, J. I., and Hol, W. G. (1998) A flash-annealing technique to improve diffraction limits and lower mosaicity in crystals of glycerol kinase, *Acta Crystallogr. D54*, 479−480.
32. Kriminski, S., Caylor, C. L., Nonato, M. C., Finkelstein, K. D., and Thorne, R. E. (2002) Flash-cooling and annealing of protein crystals, *Acta Crystallogr. D58*, 459−471.
33. Kabsch, W. (1993) Automatic processing of rotation diffraction data from crystals of initially unknown symmetry and cell constants, *J. Appl. Crystallogr. 26*, 795−800.
34. Kissinger, C. R., Gehlhaar, D. K., and Fogel, D. B. (1999) Rapid automated molecular replacement by evolutionary search, *Acta Crystallogr. D55*, 484−491.
35. Jones, T. A., Zou, J. Y., Cowan, S. W., and Kjeldgaard, M. (1991) Improved methods for building protein models in electron density maps and the location of errors in these models, *Acta Crystallogr. A47*, 110−119.
36. Perrakis, A., Harkiolaki, M., Wilson, K. S., and Lamzin, V. S. (2001) ARP/wARP and molecular replacement, *Acta Crystallogr. D57*, 1445−1450.
37. Winn, M. D., Isupov, M. N., and Murshudov, G. N. (2001) Use of TLS parameters to model anisotropic displacements in macromolecular refinement, *Acta Crystallogr. D57*, 122−123.
38. Laskowski, R. A., MacArthur, M. W., Moss, D. S., and Thornton, J. M. (1993) PROCHECK: A program to check the stereochemical quality of protein structures, *J. Appl. Crystallogr. 26*, 283−291.
39. Schuettelkopf, A. W., and van Aalten, D. M. F. (2004) PRODRG: A tool for high-throughput crystallography of protein−ligand complexes, *Acta Crystallogr. D60*, 1355−1363.

40. Kleywegt, G. J. (1996) Use of non-crystallographic symmetry in protein structure refinement, *Acta Crystallogr. D52*, 842−857.
41. Kiefersauer, R., Than, M. E., Dobbek, H., Gremer, L., Melero, M., Strobl, S., Dias, J. M., Soulimane, T., and Huber, R. (2000) A novel free-mounting system for protein crystals: Transformation and improvement of diffraction power by accurately controlled humidity changes, *J. Appl. Crystallogr. 333*, 1223−1230.
42. Jelakovic, S., and Schulz, G. E. (2002) Catalytic mechanism of CMP: 2-Keto-3-deoxy-*manno*-octonic acid synthetase as derived from complexes with reaction educt and product, *Biochemistry 41*, 1174−1181.
43. Heckmann-Pohl, D. M., Bastian, S., Altmeier, S., and Antes, I. (2006) Improvement of the fungal enzyme pyranose 2-oxidase using protein engineering, *J. Biotechnol.* (in press).
44. Muller, Y. A., Schumacher, G., Rudolph, R., and Schulz, G. E. (1994) The refined structures of a stabilized mutant and of wild-type pyruvate oxidase from *Lactobacillus plantarum*, *J. Mol. Biol. 237*, 315−335.
45. Bjørk, A., Dalhus, B., Mantzilas, D., Sirevåg, R., and Eijsink, V. G. H. (2004) Large improvement in the thermal stability of a tetrameric malate dehydrogenase by single point mutations at the dimer-dimer interface, *J. Mol. Biol. 341*, 1215−1226.
46. Meyer, M., Wohlfahrt, G., Knäblein, J., and Schomburg, D. (1998) Aspects of the mechanism of catalysis of glucose oxidase: A docking, molecular mechanis and quantum chemical study, *J. Comput.-Aided Mol. Des. 12*, 425−440.
47. Lario, P.-I., Sampson, N., and Vrielink, A. (2003) Sub-atomic resolution crystal structure of cholesterol oxidase: What atomic resolution crystallography reveals about enzyme mechanism and the role of the FAD cofactor in redox activity, *J. Mol. Biol. 326*, 1635−1650.
48. Funcke, W., and von Sonntag, C. (1979) Detection of the open-chain forms of D-fructose and L-sorbose in aqueous solution by using ^{13}C NMR spectroscopy, *Carbohydr. Res. 75*, 305−309.
49. Meyer, J. E. W., and Schulz, G. E. (1997) Energy profile of maltooligosaccharide permeation through maltoporin as derived from the structure and from a statistical analysis of saccharide-protein interactions, *Protein Sci. 6*, 1084−1091.
50. Freimund, S., Huwig, A., Giffhorn, F., and Köpper S. (1998) Rare keto-aldoses from enzymatic oxidation: Substrates and oxidation products of pyranose 2-oxidase, *Chem.—Eur. J. 4*, 2442−2455.

BI052465D